condensed matter

MDPI

Review

Perspectives of XRF and XANES Applications in Cryospheric Sciences Using Chinese SR Facilities

Wei Xu [1,*], Zhiheng Du [2,*], Shiwei Liu [2], Yingcai Zhu [1], Cunde Xiao [3] and Augusto Marcelli [4,5]

1 Beijing Synchrotron Radiation Facility, Institute of High Energy Physics, Chinese Academy of Sciences, Beijing 100049, China; yingcaizhu@ihep.ac.cn
2 State Key Laboratory of Cryospheric Science, Northwest Institute of Eco-Environment and Resources, Chinese Academy of Sciences, Lanzhou 730000, China; liushiwei1990@lzb.ac.cn
3 State Key Laboratory of Land Surface Processes and Resource Ecology, Beijing Normal University, 19 Xinjiekouwai Street, Beijing 100875, China; cdxiao@bnu.edu.cn
4 INFN-Laboratori Nazionali di Frascati, Via E. Fermi 40, 00044 Frascati (RM), Italy; marcelli@lnf.infn.it
5 RICMASS, Rome International Center for Materials Science Superstripes, Via dei Sabelli 119A, 00185 Rome, Italy
* Correspondence: xuw@mail.ihep.ac.cn (W.X.); duzhiheng10@163.com (Z.D.); Tel.: +86-010-8823-5156 (W.X.)

Received: 6 September 2018; Accepted: 29 September 2018; Published: 8 October 2018

Abstract: As an important part of the climate system, the cryosphere, can be studied with a variety of techniques based on laboratory-based or field-portable equipment in order to accumulate data for a better understanding of this portion of the Earth's surface. The advent of synchrotron radiation (SR) facilities as large scientific interdisciplinary infrastructures has reshaped the scenario of these investigations and, in particular, of condensed matters researches. Many spectroscopic methods allow for characterizing the structure or electronic structure of samples, while the scattering/diffraction methods enable the determination of crystalline structures of either organic or inorganic systems. Moreover, imaging methods offer an unprecedented spatial resolution of samples, revealing their inner structure and morphology. In this contribution, we briefly introduce the SR facilities now available in mainland China, and the perspectives of SR-based methods suitable to investigate ice, snow, aerosols, dust, and other samples of cryospheric origin from deep ice cores, permafrost, filters, etc. The goal is to deepen the understanding in cryospheric sciences through an increased collaboration between the synchrotron radiation community and the scientists working in polar areas or involved in correlated environmental problems.

Keywords: synchrotron radiation; X-ray fluorescence spectroscopy; X-ray absorption fine structure spectroscopy; trace elements; cryospheric sciences; snow; ice; dust

1. Introduction

The cryosphere was proposed as the fifth earth sphere alongside the atmosphere, hydrosphere, lithosphere, and biosphere in the ecosystem. Moreover, changes in the cryosphere may reflect global climate changes [1]. For instance, environmental water resources [2] or the pollutant mercury [3] have recently been extensively investigated in China in order to understand global climatic changes and other environmental issues.

Large synchrotron radiation facilities based on dedicated accelerators have been available to users since the early 1990s, and gained an increased interest in the new millennium. After almost six decades of operation, the scenario of synchrotron radiation is going to evolve into low-emittance and quasi-diffraction limit storage rings, either by upgrading the existing facilities (e.g., APS, ESRF,

SPring-8, Diamond, Elettra, ALS, etc.) or by building new dedicated storage rings (such as HEPS in China, SIRIUS in Brazil, MAX IV in Sweden, etc.) [4] At the same time, fourth generation sources, X-ray free electron lasers (FELs), have also been built in Europe, Japan, South Korea, the United States, and in China. These radiation sources offer novel capabilities to investigate the different states of matter from the atomic to nano- and micro-scopic scale.

The continuous increase of synchrotron radiation applications both at storage rings and FELs, in all scientific areas, such as biology, chemistry, materials science, physics, geological and environmental sciences, paleontology, cultural heritage, as well as industrial applications, were made possible by many new instrumental capabilities. In the past, user communities in each scientific area have been established by starting just one or few synchrotron radiation experimental methods. However, many opportunities still remain unexplored in different fields at SR or FEL facilities. Meanwhile, unlike bench top experimental devices, beamlines at large synchrotron radiation facilities are characterized by an Open Access policy, based on the free competition among proposals/experiments that are ranked only by looking at their scientific content at the international level. Actually, the high demand of these facilities restricts their access only to a limited number of researchers, typically running one experiment per year. Only highly competitive proposals are approved and get beamtime. Hence, it is important for each community to know the characteristics of the instruments available at the synchrotron radiation facilities in order to be competitive and successful to solve their open problems.

Cryospheric science is one of the research areas that requires these powerful sources, but at present, only a limited number of scientific researchers have had opportunities to use these infrastructures [5–9]. In this work, after a brief introduction of the various SR techniques that might be of interest for cryospheric researchers, we will address the main techniques that can be performed at Chinese synchrotron radiation facilities in this area, which is of great interest to the Chinese research communities involved in geological, environmental, climatic, and atmospheric research.

2. Synchrotron Radiation-Based Techniques

2.1. X-ray Fluorescence (XRF)-Trace Element Identification

2.1.1. Basics

X-ray fluorescence spectroscopy is based on the emission of secondary photons upon the excitation of core electrons followed by electronic transitions from higher levels to the vacancy state. In atomic physics, K, L, M, and N stand for the main shells numbered as 1, 2, 3, and 4, respectively, while the s, p, d, and f orbitals correspond to different subshells. In X-ray physics, the electron orbitals surrounding the atomic core are indexed as K, L, M, and N, while the K stands for 1s (1/2) shell, L_1 for 2s (1/2), L_2 for 2p (1/2), and L_3 for 2p (3/2). As shown in Figure 1, the X-ray fluorescence line emitted with the transition from the L to K shell is called K_α, while that for the M to K shell is called K_β. For the subshell transitions, the emission lines are named $K_{\alpha 1}$, $K_{\alpha 2}$, $K_{\beta 1}$, $K_{\beta 3}$, and so on. The M to L shell transitions are named as L_α, L_β, L_γ, and so on.

The X-ray fluorescence (XRF) lines of each element are defined by the transition energy among the different orbitals. Each line occurs at a fixed energy and the fluorescence lines are clearly separated for the different elements. The energy value of each emission line allows for identifying the element in the investigated sample. For instance, the K_α and K_β lines of iron can be detected at 6.4 keV and 7.06 keV, respectively. Meanwhile, the L_α, L_β, and L_γ lines of lead occur at 10.6 keV, 12.6 keV, and 14.8 keV, respectively. Usually, one should rely on at least two lines to verify the presence of the corresponding element, because the poor energy resolution XRF lines of some elements may overlap and cannot be distinguished using a conventional detection scheme. For instance, the K_α line of arsenic is quite close to the L_α line of lead. With an energy dispersive or a wavelength dispersive detection scheme, it is possible to distinguish the XRF lines with a high energy resolution.

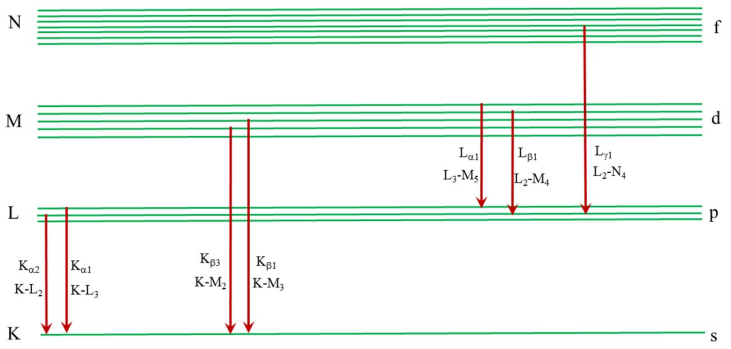

Figure 1. The nomenclature of the X-ray fluorescence lines based on the electron orbital diagram.

2.1.2. Synchrotron Radiation X-ray Fluorescence

A typical synchrotron radiation XRF experimental setup consists of an intense radiation source (bending magnets or an insertion device like a wiggler or an undulator), a transport line that deflects and focuses the X-ray beams, and the end-station where experiments can be performed. Usually, SR-XRF provides a tiny focused beam with a spot size ranging from tens of nanometers up to tens of micrometers, depending on the optical configurations. Some beamlines may offer a spot of variable sizes to fulfill the different experimental demands [10]. In the experimental station, the focused beam is delivered onto the sample and excited fluorescence photons are emitted. To eliminate the strong Compton scattering contribution, the detection geometry has the detector set at 90°, while the sample is set at 45° with respect to the incident beam.

For X-ray fluorescence measurements, one should be concerned about photons illuminating the samples, which will affect the detection limit and the measuring time. There are two classes of experiments that require intense and brilliant synchrotron radiation sources. The first looks at the reconstruction of the spatial heterogeneity in the sample under investigation, and in particular, the mapping of the spatial distribution of the chemical elements. For this type of measurement, we need to carefully evaluate the time necessary to scan the sample area according to spatial resolution and signal to noise (S/N) ratio. For instance, a map 1×1 mm^2 can take several hours using a 5 μm spot with 1 s of acquisition at each point. Another class of SR-XRF experiments looks at elements in trace, that is, at a low and ultralow detection limit, which could be as low as the μg/g level. It should be noted that the absolute detection limit in the mass can reach *fg* and possibly *ag*. These detection values are now possible only at synchrotron radiation beamlines, and the advantage of measuring trace elements with this technique is that it is both highly sensitive and non-destructive. It allows for further analytical techniques to be performed on the same sample. Meanwhile, it should be noted that the total reflection XRF (TXRF) technique that works in the grazing incidence geometry is very well suited for trace-element studies in aqueous solutions, and was successfully applied to investigate the aeolian dust in Antarctica and Alpine deep ice cores [7].

Presently, we have two powerful beamlines at Chinese synchrotron facilities where XRF experiments can be performed, namely: the 4W1B beamline at the Beijing Synchrotron Radiation Facility (BSRF) and the BL15U at the Shanghai Synchrotron Radiation Facility (SSRF) [11]. The first works in the wide bandwidth mode using a double monolayer monochromator, while the second works with the narrow bandwidth mode using a double crystal monochromator. The main working energy at 4W1B is 15 keV, while the X-ray beam is focused down to 20–50 μm in diameter by using a polycapillary lens. However, the energy can be tuned in the range of 5–20 keV and the X-ray beam can be focused down to 2×2 μm^2 by using a couple of Kirkpatrick-Baez mirrors. Users can select the corresponding beamline according to their specific purpose and requirements. The XRF spectra can be fitted to a obtain quantitative evaluation of the elemental concentration by means of calibration curves, using certified standards. The software package PyMCA [12], developed by the European Synchrotron Radiation Facility, is available and is commonly used for data reduction and analysis.

2.2. X-ray Absorption Spectroscopy (XAS)-Atomic Structural Information

In X-ray spectroscopy (XAS), photons excite bound electrons in the atomic core levels (core electrons) to the unoccupied states in the continuum above the Fermi level. The atomic absorption cross-section shows typical step-like jumps at the energy of the core electrons' binding energy. The first interpretation of the modulation of the atomic cross-section over about the 1000 eV photon energy range beyond the absorption edge, was proposed by R.L. Kronig [13], and it was confirmed by using the synchrotron radiation [14], which provides a unique continuum spectrum from the soft to the hard X-ray range. These spectral features are called the "Kronig structure" [13], and since 1970, have used the acronym EXAFS (extended X-ray absorption fine structure) [14]. In this regime, the oscillation of the absorption cross-section is due to the scattering of the fast photoelectron by neighbor atoms confined within the single scattering regime, because of the weak backscattering probability for a fast, high energy photoelectron. The strong sharp absorption peaks appearing in the first hundred eV energy range beyond the absorption edge have been the object of long standing discussions and controversy, generating significant confusion in the literature, as in this energy range the photoelectron energy is small, and therefore the excited photoelectron has a very large scattering cross-section interacting with the neighbor atoms, and its wave-length is much larger than the interatomic distances, thus the single scattering EXAFS approximation is not valid. Moreover, the lifetime of the excited photoelectron is short and its mean free path is also limited, therefore the final short living states are confined to the nanoscale. In 1974, it was proposed that the strong absorption peaks near the absorption edge are due to quasi stationary states of the excited photoelectron degenerate with the continuum localized by strong multiple scattering [15], and it was confirmed experimentally first in disordered aluminum oxide [16], nitrogen gas [17], biological matter [18], surface oxides [19], and complex transition metal oxides, where the acronym XANES (X-ray absorption near edge structure) was proposed [20], in order to indicate the final states localized on the nanoscale by multiple scattering by the atoms surrounding the photo-absorber.

XANES [14] is a widely used probe of both the local structure at an atomic scale, and the electronic structure. X-rays excite core-level electrons and the photoelectrons are scattered by the atoms surrounding the photo-absorber. The scattering of the excited electrons allows for local structural information, such as electronic and geometric structures, to be extracted. XRF and XAS use the same nomenclature, for example, the K-shell electron is excited (K absorption edge appears in XAS spectrum), then K_α or K_β are the characteristic emission lines in the XRF spectrum. It is worth mentioning that the XAS spectra can be measured by the transmission or fluorescence mode. For the fluorescence detection mode, one should measure the emitted fluorescence lines by scanning the incident energy across the absorption edge. To interpret XAS data, one has to separate the entire spectrum into two regions, namely: the first from 50 eV before up to 60–80 eV (depending on the system and also coordination and bond distances) above the absorption edge, which is called XANES (X-ray absorption near-edge spectroscopy); the second after the XANES region up to 1000 eV or more (depending on the S/N ratio), which is called the EXAFS (extended X-ray absorption fine structure spectroscopy) region [21]. Although one can get both the XANES and EXAFS spectra in one measurement, the interpretation of the XANES and EXAFS spectra are different, and they contain different information. For the XANES spectra, one can obtain the electronic structure and the local geometrical structure (i.e., coordination and bond angles) surrounding the selected absorber atom. By contrast, EXAFS is extremely useful for obtaining the coordination number, the bond distance, and the mean-square-relative displacement of the bonded atoms, through model-based fits. Although both XANES and EXAFS can be interpreted using the multiple scattering theory [10,11], the first is based only on the multiple scattering (MS) analysis in the real space, while the second mainly probes single scattering (SS) events. The EXAFS interpretation requires structural fitting, while the XANES spectra, in addition to simple fingerprinting, can be successfully used to obtain quantitative structural information based on the fitting [22]. Several software packages for the data analysis and interpretations are now available, namely:

(1) IFEFFIT and Demeter package for data reduction and EXAFS fittings [23];
(2) Full multiple scattering calculations implemented in FEFF [24] and FDMNES [25] are commonly employed for simulating XANES spectra; and
(3) XANES fitting as implemented in MXAN [22,26], is based on the comparison between the experimental spectrum and several theoretical calculations generated by changing the relevant geometrical parameters of the site by calculating each configuration with full multiple scattering theory.

2.3. Other Synchrotron Radiation Techniques and Beyond

In addition to XRF and XAFS, it is important to mention that other techniques available at synchrotron radiation facilities may offer important opportunities for cryospheric and environmental researches. Nowadays, several high-energy resolution fluorescence detection mode XANES facilities are available and allow one to measure the near-edge region with more detail [27]. Also, the X-ray diffraction method, a well-established technique that reveals the crystalline structure of organic and inorganic samples with a long-range structural order is available at SR facilities. SR-XRD offers a much faster and more accurate structural refinement than any conventional source on samples of extremely small dimensions (down to micrometer size), so even the analysis of single grains or particulate matter (PM) is possible [28]. Finally, the X-ray tomography can be also used to collect unique 3D images of the internal structure of a sample with an extremely high spatial resolution and a high absorption or phase contrast [29,30]. In the next section, we will briefly illustrate some applications of the different techniques used in environmental sciences, which are of great interest to cryospheric researches.

3. Experimental Applications

3.1. Spectroscopic Methods

Mercury is a global pollutant whose environmental importance steams from its extreme mobility and toxicity. In order to understand its biogeochemical cycle, also in relation to human disturbances, it is important to assess the emitting sources; the dynamics, which govern its transport through the atmosphere; and the deposition on continents and oceans. Primary anthropogenic Hg emissions greatly exceed natural geogenic and biogenic sources, resulting in a massive disturbance of its cycle on a global scale [31]. Moreover, the toxicity is one of the main concerns in biology, and the chemical speciation is extremely useful to monitor and limit the toxicity effects induced by heavy elements such as mercury. Recently, Li et al. [32] investigated the famous Tibetan medicine called Zuotai, which has been used for treating various diseases for over 1300 years, and is still used in some areas in the Tibetan Plateau. These drugs contain mercury and, counter intuitively, they are not toxic. Zuotai was proven effective in treating inflammations, anthrax, and so on. To understand the mechanisms beyond the Tibetan medicine, Li et al. [8] investigated the chemical speciation as well as the distribution of mercury in the organs of treated animals, by combining the μ-XRF and XANES techniques. By comparing the XANES spectra at Hg L_3-edge for Zuotai and other reference mercury compounds, they recognized $HgCys_2$ and MeHgCys as the mercury compounds present in the organs. By using μ-XRF imaging with a 200 μm spatial resolution, they also revealed that mercury is accumulated in the renal cortex of the kidney. Moreover, the mercury deposition in the kidneys treated with Zuotai is much less than those treated by feeding β-HgS or $HgCl_2$ (Figure 2). The speciation of Hg was revealed with a linear combination fitting with reference to the Hg L_3-edge XANES spectra, and most of the Hg^{2+} ions were bounded to the sulfydryl group, which is less toxic. From this study, we learnt that both the microscopic distribution and the bond nature of Hg ions are important in order to understand the toxicity and the transport mechanisms of Hg in biological systems.

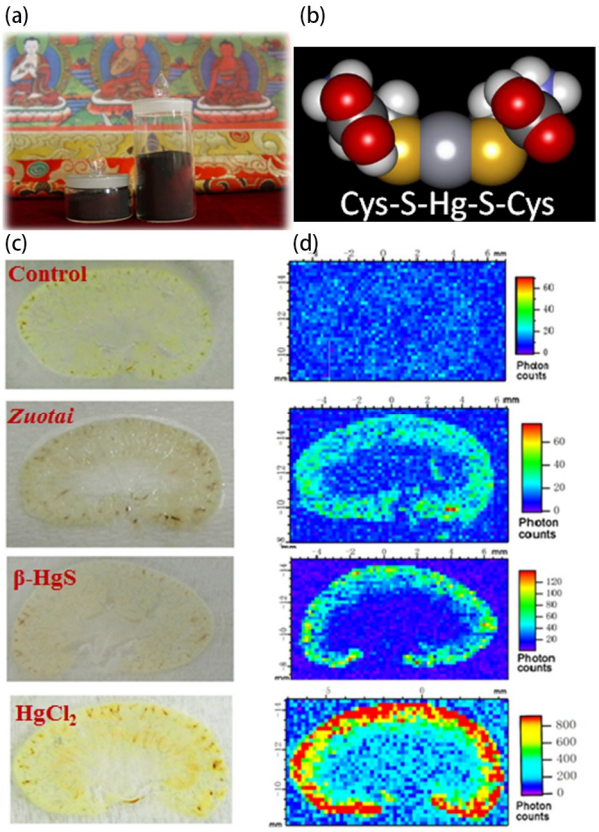

Figure 2. (**a**) Photo of the Tibetan medicine Zuotai; (**b**) molecular scheme of the $HgCys_2$; (**c**) images of slices of kidney from mice untreated and mice treated with Zuotai, β-HgS, or $HgCl_2$, respectively; (**d**) maps of the mercury distribution using μ-X-ray fluorescence (XRF) (figures redrawn from the literature [32] and with courtesy of Cen Li).

The consumption of fish, fish products, and marine mammals is generally considered to be the main global pathway of human exposure to methylmercury (MeHg). Soil is the primary source of MeHg exposure to rice plant tissues. By using the μ-XRF and XANES spectra at the Hg L_3-edge, Meng et al. [33] investigated the distribution and speciation of mercury in three fractions of the rice grains (hull, bran, and white rice), collected from an Hg-contaminated region in China. The majority of the inorganic mercury (IHg) in a rice grain is found in the hull and bran (Figure 3). However, the majority of the toxic species, the methyl mercury (MeHg), is found in edible white rice. This study revealed that the transport of mercury due to anthropic activities is extremely sophisticated. Identifying the atomic coordination of mercury may provide a clue for figuring out a better solution to fix or minimize pollution issues. By employing the high-energy resolution XANES (HR-XANES) spectra [27,34–37] with the fluorescence detection method, Manceau et al. obtained fine details in the near-edge region at the Hg L_3-edge. Combining the theoretical simulations, the bonding nature of the mercury compounds in the environment was investigated with more physical insights [36,37]. A key link between the inorganic Hg input and exposure of humans and wildlife is the net production of methyl-mercury, one of the most dangerous Hg species with regards to toxicity issues. It is mainly produced in the anoxic zones of freshwater, terrestrial, and coastal environments, and in the deep part of the ocean [38]. Climate change is occurring across the world, and in this context, high latitude and altitude regions are particularly fragile, where climate change is advancing faster than in other regions.

The Tibetan Plateau (TP) is the highest and largest highland in the world, with an average elevation of over 4000 m above sea level (a.s.l.). The permafrost body in the TP is the largest permafrost region at low- and mid-latitudes, and accounts for 74.5% of the Northern Hemisphere's mountain permafrost. Presently, limited studies on Hg behaviors (e.g., distribution, variation, etc.) have been performed

in high-altitude permafrost regions [39], and, to the best of our knowledge, the influencing factors on Hg behavior in the frozen soils of the permafrost regions have been poorly studied. Moreover, only few studies have reported concentrations and distribution of Hg in the surface soils of the TP. Hg concentrations are typically extremely low, and attempts to measure the Hg K characteristic lines are needed. Although challenging, this approach is strategic to probe the Hg amount in soils and to understand how chemical mechanisms may occur in different regions. Moreover, it is also important to investigate how the different Hg species are transported, transformed, and accumulated at local and global scale.

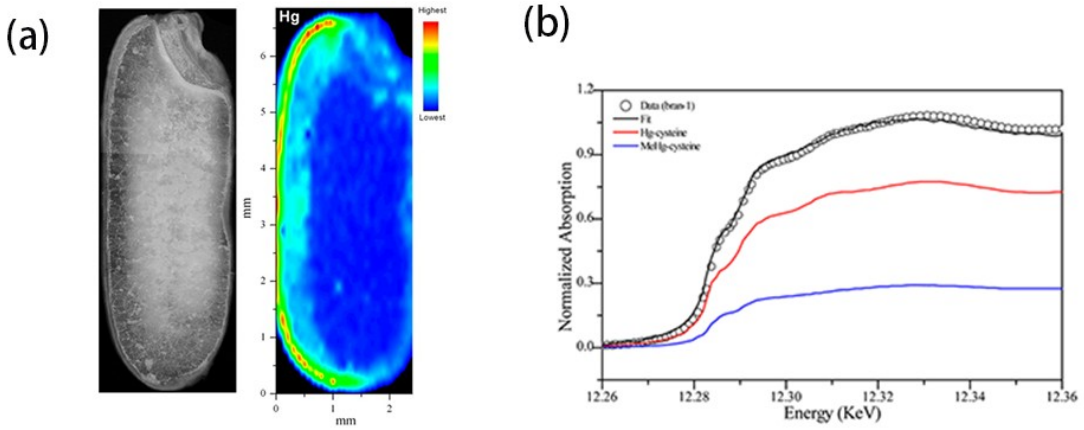

Figure 3. (**a**) Comparison of the optical image with the μ-XRF image and (**b**) comparison of the X-ray absorption near-edge spectroscopy (XANES spectra) of a grain of rice, as well as the reference standards (figures redrawn from the literature [33]). Reprinted with permission from [33]. Copyright {2014} American Chemical Society.

3.2. Spectroscopy and Incineration of Waste

The dust and aerosols originate from the solid particles and/or liquid droplets emitted, as well as the secondary particles that are formed via chemical reactions in the atmosphere. Municipal solid waste (MSW) refers to the trash or garbage from homes, schools, and hospitals, as well as products such as packaging, furniture, clothing, bottles, newspapers, appliances, batteries, and so on. Environmental pollution can be associated with MSW.

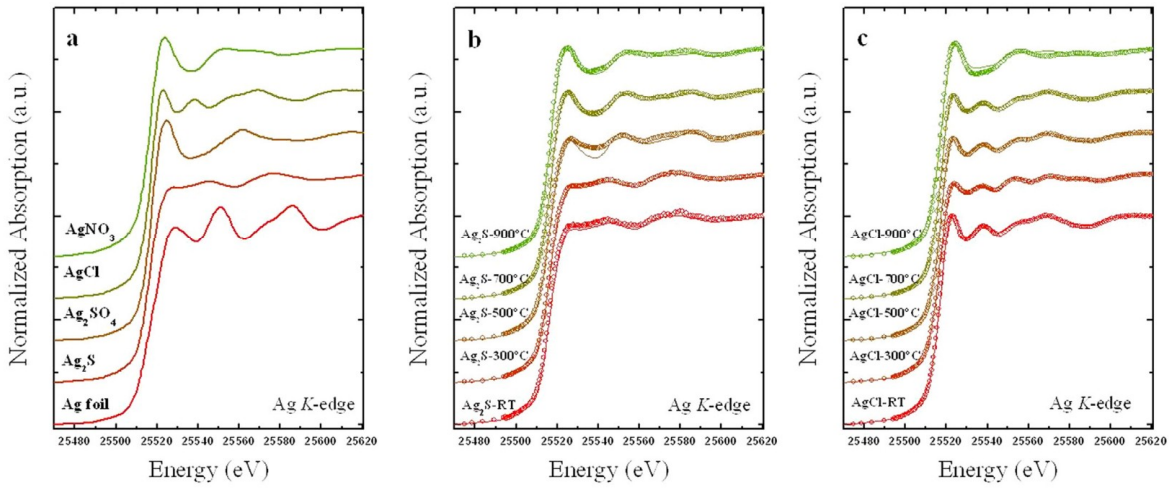

Figure 4. The linear combination fit of the temperature dependent XANES spectra at the Ag *K*-edge: (**a**) reference spectra of reference compounds; (**b**) Ag_2S spiked sludge; and (**c**) AgCl spiked simulated municipal solid waste (SMSW). See the text for more details (figure redrawn from the literature [41]).

For instance, burning waste coal can generate hazardous matter, with serious health risks for human beings [40]. It is essential to retrace the origin of these pollutants and to figure out an approach to reduce the amount of hazardous contents. To identify the chemical reactions occurring in the treatment of industrial waste, Yin et al. [41] investigated the chemical transformation of AgCl and Ag_2S in silver nanoparticles under sunlight or incineration. By using the linear combination fitting of the Ag K-edge XANES spectra of Ag_2S spiked sludge and AgCl spiked simulated municipal solid waste (SMSW) incinerated at various temperatures and with certain protocols, it was pointed out that chemical transformations of Ag_2S and AgCl into elemental silver could be a source of Ag nanoparticles (See Figure 4).

Municipal solid waste incineration (MSWI) is a widespread method to treat MSW, and fly ash can be produced in this process. At variance, the secondary fly ash (SFA) is due to a secondary chemical reaction occurring with condensation after vaporization, during the flue gas cooling procedure. The latter is a reusable material suitable for the construction industry to produce bricks. Hence, it is fundamental to investigate the speciation of toxic heavy metals using XAFS. In the SFA samples, Tian et al. [42] revealed that lead mainly existed as $PbCl_2$ and PbS, while PbO and $PbCl_2$ can be identified in MSWI fly ash using a linear combination fitting of the XANES spectra. By using the EXAFS fitting, they also reconstructed the geometrical structure around lead. This study underlines how the structural information is important for optimizing the recycling process of municipal solid waste.

3.3. Applications of Tomography in Environmental Research

Three-dimensional imaging using X-ray micro-computed tomography enables the visualization and quantification of the brine network morphology and variability [43,44]. Duplicate scans have been performed using X-ray energies above and below the absorption edge of the interested elements, using a synchrotron radiation source, which provides monochromatic radiation and a highly tunable beam at variable X-ray energy. Synchrotron radiation X-ray tomography based on absorption contrast enables a clear discrimination of air, ice, and solid salts, if the contained elements have a drastic mass difference. For instance, the internal structure of sea ice samples, shown in Figure 5, can be observed with a strong contrast [45], as follows: air (dark), ice (grey), and salt crystals or brine (white). The field of view was about 12 mm, while the voxel size was 5.6 µm [45]. With the improved algorithms and the advances in X-ray tomography, one can obtain a qualitative estimation of the pore size, and so on, which could be useful to estimate the motion of the glacier [46]. Furthermore, the tomography method can be successfully used to study clathrate gas hydrates [45,47–49], ice and clathrate [50], plant roots and soils [51], aerosols [52], and so on.

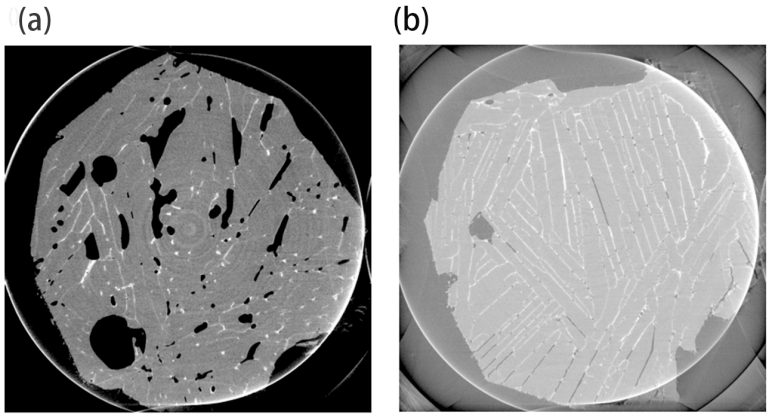

Figure 5. Images of a horizontal slice of a sea ice sample: (**a**) as grown and (**b**) rapidly cooled, as measured by SR tomography at about −30° C (figures redrawn from the literature [45]).

4. Perspectives in Applications of SR Techniques in Cryospheric Sciences

In many cryospheric researches, even the sampling and its preservation are challenging. Samples to characterize and understand the atmosphere, the climate evolution, and the status of the Earth's ecosystem are rare and extremely precious. Actually, airborne particles and dust are generated and transported over time by natural mechanisms and by human related activities. During transport, the elements may experience different thermodynamical conditions, and chemical reactions may occur, affecting the speciation of many elements. To recognize the source as well as the evolution pathways, synchrotron radiation techniques represent a powerful and unique tool. Although a limited number of publications [5–9] in this field have used synchrotron radiation techniques, efforts to expand the number of applications will certainly be beneficial to trigger new researches and to expand the community working in cryospheric science. Indeed, ice and snow are key elements of the cryosphere; ice is central to climate, geology, and life. Understanding its behavior on Earth is essential for predicting the future of the planet and unraveling the emergence of life in the universe [53–56]. Although challenging, the following research opportunities using synchrotron radiation techniques are extremely promising:

(1) trace elemental analysis in deep ice core. By applying SR-XRF, it is possible to obtain quantitative information about the elemental concentration without damaging the sample. However, for ultra-trace analysis, it is important to the protect samples under investigation from external contaminations. Specially designed sample chambers installed at end-stations are required. To reach ultra-low detection limits with the highest S/N ratio, the highest flux at the sample position and the best detectors are necessary;

(2) the speciation of metals, as illustrated in the previous examples, is possible through performing XANES experiments. However, it is necessary to concentrate the investigated elements, and sample preparation is a key issue [57,58]. This is a particularly important to investigate the inorganic fraction contained in the deep ice core [59]. In this case, it is necessary to melt from several centimeters up to meters of ice core to reach the detection limit. Moreover, a spectral database should be established with as many standards as possible to identify the chemical reactions that might occur. A mimicking in situ XANES measurement under different sample conditions (gas, temperature, etc.) would also help to understand the reaction pathways of the different elements induced by climatic changes or anthropogenic activities;

(3) establish the largest possible dataset by measuring samples from the entire ecosystem extending over time and regions. Statistics will be helpful to draw more reliable conclusions. Hence, in order to describe climatic changes, one needs to sample the entire ecosystem, including, but not limited to, ice, snow, aerosols, dust, soils, solid state waste, and so on.

The introduction of new SR techniques and overcoming technical issues are always possible. We need to focus on the emerging techniques so as to investigate at the best overall physical–chemical processes occurring in the cryosphere and in its components (air, water, snow, ice, and permafrost). There are many difficulties that have limited experimental research in this field, but they can be overcome with a synergic effort among scientists and researchers working in these large infrastructures. As shown in Table 1, there are already some beamlines that can offer the XRF, XAFS, XRD, and tomography at current synchrotron radiation facilities in Beijing, Shanghai, and Hefei. The construction of new beamlines in an SSRF upgrade and in planned HEPS would expand the capabilities in many aspects, such as the energy/spatial resolution and integration of different techniques. The community of cryospheric science needs to know the opportunities and contribute.

Table 1. Techniques available at Chinese Synchrotron Facilities * in the mainland of China.

Synchrotron Radiation Facility	Beamline	Availability	Energy (keV)	Focal Spot (V × H μm)	Technique
Beijing Synchrotron Radiation Facility (BSRF)	4W1B	Operation	5–20	20 × 20	μ-XRF
	1W1B	Operation	4–23	900 × 300	XAFS
	1W2B	Operation	5–20	1000 × 600	XAFS
	4B7A	Operation	2.1–5.7	3000 × 1000	XAFS, calibration
	4B9A	Operation	4–15	2000 × 1000	XRD, XAFS,
	4W1A	Operation	6–22	20000–10,000	CT
			5–12	15 × 15	Nano-CT
Shanghai Synchrotron Radiation Facility (SSRF)	BL15U1	Operation	5–20	1.6 × 1.8 (variable) using KB 0.15 × 0.15 using zone plate	μ-XRF μ-XAFS μ-XRD
	BL14W1	Operation	4.5–35	300 × 300	XAFS
	BL14B1	Operation	4–22	400 × 400	XRD
	BL13W1	Operation	8–72.5	45,000 × 5000	CT
Shanghai Synchrotron Radiation Facility (SSRF) Upgrade	E-line	Construction	1.3–10	80 × 200	XPS, XAFS
	D-line	Construction	5–25 (X-ray)	NA	XAFS, FTIR
			$10–10^4$ cm^{-1} (IR)	100 × 100	
	Tender beamline	Construction	2.1~16	5 × 1.5	XAFS
	General spectroscopy	Construction	5–30	500 × 100	XAFS
	Nanobeamline	Construction	5–25	0.01 × 0.01	
National Synchrotron Radiation Laboratory (NSRL)	BL01B	Operation	15–4000 cm^{-1}	NA	FTIR
High Energy Photon Source (HEPS)	BD	Planning	2.1–7.8	400 × 400	XAFS
	BE	Planning	5–15	NA	Tomography
	B2	Planning	5–25	0.009 × 0.009	n-XRF/n-XRD
	B5	Planning	5–25	10 × 10	XRS, NRS, RIXS
	B8	Planning	4.8–45	NA	QXAFS

* BSRF and HEPS are both in Beijing, SSRF in Shanghai, and NSRL in Hefei; * Other sources have been proposed in China, but at present no precise data are available.

5. Relevance of Cryospheric Sciences to Synchrotron Radiation in China

Synchrotron radiation techniques may offer several opportunities in cryosphere and environmental sciences, because of their high resolution and reliability. Chinese scientists first used synchrotron radiation to analyze algae, lichen, bryophyte, and Adelie penguins from Antarctica [60–62]. These early works promoted polar environmental researches at the micro level. The X-ray fluorescence method is extremely powerful to investigate the role of heavy metals on polar species. This method has been also applied in an Arctic aerosol research [63]. Samples of aerosols from the marine boundary layer of the Arctic Ocean were collected aboard the R/V Xuelong on the Second Chinese Arctic Research Expedition (July–September 2003), and the chemical composition of these particles was determined using SR-XRF.

Mercury is a global pollutant that affects human and ecosystem health. In the last two decades, anthropogenic Hg emissions declined in Europe, but significantly increased in Asia [64,65]. This represents a relevant issue for the Arctic region. Many studies also discussed the toxicity of Hg, which is released in the food chain as glaciers retreat. Because high amounts of Br/Cl and O_3 species will react with Hg from atmosphere, the increasing of Hg at the snow surface occurs when atmospheric mercury depletion events occur. Many data have pointed out that snow pack and melt water are the major reservoirs of atmospherically deposited mercury [66,67]. The inductively coupled plasma mass spectrometry (ICP-MS) and general mass spectrometry methods are powerful, but return limited information because they may only measure the total amount of Hg in ice cores. Moreover, this technique does not recognize elemental Hg from $MeHg^+$ and Hg^{2+} [68]. Information on other speciation mechanisms is also lacking. Moreover, the intensity of the solar radiation is very different in Arctic compared with other regions like the Tibet area. By contrast to the polar day in Arctic, a much stronger solar irradiation occurs at the high altitude of the Tibet Plateau. SR studies may allow for a more precise characterization of Hg speciation, pointing out the different reduction and oxidation conditions. Presently, the molecular mechanisms (e.g., molecular Cl and B) beyond these processes are largely unknown [69,70], and reliable knowledge of the chemical reactions in ice and snow is lacking [64]. Actually, the mercury concentration in these samples is extremely low and hard to be detected by a conventional setup. Nevertheless, the improvement of the source brilliance and multi-element detectors will certainly enable the detection of Hg down to the *ng/g* level or lower, to reach the expected values of the natural concentration. Moreover, it is necessary to establish protocols for sample filtering and concentrating, so as to perform XANES spectroscopy experiments on the same samples. These protocols are essential in order to minimize the possible contamination of these precious samples during the experiments. Hence, special sample handling systems should be implemented at dedicated beamline end-stations. Within this framework and the synergic effort among researchers and synchrotron radiation scientists, this interdisciplinary community will be able to investigate more and more samples in the existing as well as in future Chinese light sources.

6. Conclusions

In this contribution, we reviewed some applications of XRF and XAFS techniques in environmental and cryospheric sciences. The trace-element analysis and/or the mapping are now possible using synchrotron radiation. XRF allows for identify the origin and distribution of many elements of interest, ranging from low (Na, Mg, etc.) to high Z elements. Spectroscopic methods such as the XAFS technique offer a new perspective on the speciation of elements, a condition that may affect the biological functioning of many systems, and the environmental release or particulate matters. Furthermore, high-energy resolution spectroscopy may reveal detailed spectral features that could be used to better investigate and recognize the nature of many atomic bonds. Finally, new powerful imaging methods, such as X-ray tomography, could provide three-dimensional views of the internal structure of many systems, including ice and clathrate systems.

Presently, the applications of synchrotron radiation techniques in cryospheric sciences are still limited, although some recent publications [5–9] and workshops [59,71] demonstrated that the

cooperation among scientists working in cryospheric sciences and synchrotron radiation researchers is possible and extremely useful [65]. An enhanced collaboration is foreseen and efforts are necessary to make this highly interdisciplinary research area mature in order to advance the frontiers of this challenging discipline. The role of Chinese facilities and scientists will be certainly important in the next years [72].

Author Contributions: Z.D., A.M., W.X., and C.X. designed the study. Z.D., W.X., A.M., S.L., and Y.Z. carried out the synchrotron radiation experiments at BSRF, ESRF, Diamond, and ALBA over the years. W.X., A.M., S.L., and Z.D. wrote the manuscript with contributions from all of the authors.

Funding: This work was supported by the National Natural Science Foundation of China (grant No. U1532128, no. 41425003, and no. 41701071)

Acknowledgments: W.X. acknowledges the financial support and the hospitality of LNF under the framework of IHEP and INFN collaboration. W.X is grateful to Cen Li, Bo Meng, Yongguang Yin, and Jiating Zhao for sharing their ideas and insightful discussions. We strongly acknowledge the staff of the Italian CRG LISA for their support at ESRF within the experiment 08-01-1031 on Beamline BM08, and for many fruitful discussions.

Conflicts of Interest: No conflicts of interest.

References

1. Qin, D.; Ding, Y.; Xiao, C.; Kang, S.; Ren, J.; Yang, J.; Zhang, S. Cryospheric science: Research framework and disciplinary system. *Natl. Sci. Rev.* **2018**, *5*, 255–268. [CrossRef]
2. Zhang, X.; Li, H.; Zhang, Z.; Wu, Q.; Zhang, S. Recent glacier mass balance and area changes from dems and landsat images in upper reach of shule river basin, northeastern edge of tibetan plateau during 2000 to 2015. *Water* **2018**, *10*, 796. [CrossRef]
3. Yin, X.; Kang, S.; de Foy, B.; Ma, Y.; Tong, Y.; Zhang, W.; Wang, X.; Zhang, G.; Zhang, Q. Multi-year monitoring of atmospheric total gaseous mercury at a remote high-altitude site (nam co, 4730ma.S.L.) in the inland tibetan plateau region. *Atmos. Chem. Phys.* **2018**, *18*, 10557–10574. [CrossRef]
4. Jiang, X.; Wang, J.; Qin, Q.; Dong, Y.; Sheng, W.; Cheng, J.; Xu, G.; Hu, T.; Deng, H.; Chen, F.; et al. The chinese high-energy photon source and its r&d project. *Synchrotron Radiat. News* **2014**, *27*, 27–31.
5. Marcelli, A.; Hampai, D.; Cibin, G.; Maggi, V. Local vs global climate change: Investigation of dust from deep ice cores. *Spectrosc. Eur.* **2012**, *24*, 12–17.
6. Marcelli, A.; Cibin, G.; Hampai, D.; Maggi, V. Mineralogical characterization of the inorganic component from deep ice core samples: A challenging xanes investigation. *IXAS Res. Rev.* **2012**, *8*. Available online: https://www.ixasportal.net/ixas/index.php?option=com_content&view=article&id=23&Itemid=373# (accessed on 30 September 2018).
7. Cibin, G.; Marcelli, A.; Maggi, V.; Sala, M.; Marino, F.; Delmonte, B.; Albani, S.; Pignotti, S. First combined total reflection X-ray fluorescence and grazing incidence X-ray absorption spectroscopy characterization of aeolian dust archived in antarctica and alpine deep ice cores. *Spectrochim. Acta Part B At. Spectrosc.* **2008**, *63*, 1503–1510. [CrossRef]
8. Marcelli, A.; Hampai, D.; Giannone, F.; Sala, M.; Maggi, V.; Marino, F.; Pignotti, S.; Cibin, G. Xrf-xanes characterization of deep ice core insoluble dust. *J. Anal. At. Spectrom.* **2012**, *27*, 33–37. [CrossRef]
9. Ventura, G.D.; Marcelli, A.; Bellatreccia, F. Sr-ftir microscopy and ftir imaging in the earth sciences. *Rev. Min. Geochem.* **2014**, *78*, 447–479. [CrossRef]
10. Obbard, R.W.; Lieb-Lappen, R.M.; Nordick, K.V.; Golden, E.J.; Leonard, J.R.; Lanzirotti, A.; Newville, M.G. Synchrotron X-ray fluorescence spectroscopy of salts in natural sea ice: Sxrf of salts in natural sea ice. *Earth Space Sci.* **2016**, *3*, 463–479. [CrossRef]
11. Zhang, L.L.; Yan, S.; Jiang, S.; Yang, K.; Wang, H.; He, S.; Liang, D.X.; Zhang, L.; He, Y.; Lan, X.Y.; et al. Hard X-ray micro-focusing beamline at ssrf. *Nucl. Sci. Tech.* **2015**, *26*, 060101–060107.
12. Solé, V.A.; Papillon, E.; Cotte, M.; Walter, P.; Susini, J. A multiplatform code for the analysis of energy-dispersive X-ray fluorescence spectra. *Spectrochim. Acta Part B At. Spectrosc.* **2007**, *62*, 63–68. [CrossRef]
13. Hartree, D.R.; Kronig, R.D.; Petersen, H. A theoretical calculation of the fine structure for the k-absorption band of ge in gecl4. *Physica* **1934**, *1*, 895–924. [CrossRef]

14. Rehr, J.J.; Albers, R.C. Theoretical approaches to X-ray absorption fine structure. *Rev. Mod. Phys.* **2000**, *72*, 621–654. [CrossRef]
15. Dill, D.; Dehmer, J.L. Electron-molecule scattering and molecular photoionization using the multiple-scattering method. *J. Chem. Phys.* **1974**, *61*, 692–699. [CrossRef]
16. Balzarotti, A.; Bianconi, A.; Burattini, E.; Grandolfo, M.; Habel, R.; Piacentini, M. Core transitions from the al 2p level in amorphous and crystalline Al_2O_3. *Phys. Status Solidi (B)* **1974**, *63*, 77–87. [CrossRef]
17. Bianconi, A.; Petersen, H.; Brown, F.C.; Bachrach, R.Z. K-shell photoabsorption spectra of N_2 and N_2O using synchrotron radiation. *Phys. Rev. A* **1978**, *17*, 1907–1911. [CrossRef]
18. Bianconi, A.; Doniach, S.; Lublin, D. X-ray ca k edge of calcium adenosine triphosphate system and of simple ca compunds. *Chem. Phys. Lett.* **1978**, *59*, 121–124. [CrossRef]
19. Bianconi, A. Core excitons and inner well resonances in surface soft X-ray absorption (ssxa) spectra. *Surface Sci.* **1979**, *89*, 41–50. [CrossRef]
20. Belli, M.; Scafati, A.; Bianconi, A.; Mobilio, S.; Palladino, L.; Reale, A.; Burattini, E. X-ray absorption near edge structures (xanes) in simple and complex mn compounds. *Solid State Commun.* **1980**, *35*, 355–361. [CrossRef]
21. Benfatto, M.; Natoli, C.R.; Bianconi, A.; Garcia, J.; Marcelli, A.; Fanfoni, M.; Davoli, I. Multiple-scattering regime and higher-order correlations in X-ray-absorption spectra of liquid solutions. *Phys. Rev. B* **1986**, *34*, 5774–5781. [CrossRef]
22. Longa, S.D.; Arcovito, A.; Girasole, M.; Hazemann, J.L.; Benfatto, M. Quantitative analysis of X-ray absorption near edge structure data by a full multiple scattering procedure: The fe-co geometry in photolyzed carbonmonoxy-myoglobin single crystal. *Phys. Rev. Lett.* **2001**, *87*, 155501–155504. [CrossRef] [PubMed]
23. Ravel, B.; Newville, M. Athena, artemis, hephaestus: Data analysis for X-ray absorption spectroscopy using ifeffit. *J. Synchrotron Radiat.* **2005**, *12*, 537–541. [CrossRef] [PubMed]
24. Ankudinov, A.L.; Ravel, B.; Rehr, J.J.; Conradson, S.D. Real-space multiple-scattering calculation and interpretation of X-ray-absorption near-edge structure. *Phys. Rev. B* **1998**, *58*, 7565. [CrossRef]
25. Joly, Y. X-ray absorption near-edge structure calculations beyond the muffin-tin approximation. *Phys. Rev. B* **2001**, *63*. [CrossRef]
26. Benfatto, M.; Della Longa, S. Geometrical fitting of experimental xanes spectra by a full multiple-scattering procedure. *J. Synchrotron Radiat.* **2001**, *8*, 1087–1094. [CrossRef] [PubMed]
27. Manceau, A.; Lemouchi, C.; Enescu, M.; Gaillot, A.-C.; Lanson, M.; Magnin, V.; Glatzel, P.; Poulin, B.A.; Ryan, J.N.; Aiken, G.R.; et al. Formation of mercury sulfide from hg(ii)–thiolate complexes in natural organic matter. *Environ. Sci. Technol.* **2015**, *49*, 9787–9796. [CrossRef] [PubMed]
28. Török, S.; Faigel, G.; Jones, K.W.; Rivers, M.L.; Sutton, S.R.; Bajt, S. Chemical characterization of environmental particulate matter using synchrotron radiation. *X-ray Spectrom.* **1994**, *23*, 3–6. [CrossRef]
29. Momose, A.; Takeda, T.; Itai, Y.; Hirano, K. Phase-contrast X-ray computed tomography for observing biological soft tissues. *Nat. Med.* **1996**, *2*, 473–475. [CrossRef] [PubMed]
30. Munro, P.R.T.; Ignatyev, K.; Speller, R.D.; Olivo, A. Phase and absorption retrieval using incoherent X-ray sources. *Proc. Natl. Acad. Sci. USA* **2012**, *109*, 13922. [CrossRef] [PubMed]
31. Sen, I.S.; Peucker-Ehrenbrink, B. Anthropogenic disturbance of element cycles at the earth's surface. *Environ. Sci. Technol.* **2012**, *46*, 8601–8609. [CrossRef] [PubMed]
32. Li, C.; Xu, W.; Chu, S.; Zheng, Z.; Xiao, Y.; Li, L.; Bi, H.; Wei, L. The chemical speciation, spatial distribution and toxicity of mercury from tibetan medicine zuotai, β-hgs and hgcl2 in mouse kidney. *J. Trace Elem. Med. Biol.* **2018**, *45*, 104–113. [CrossRef] [PubMed]
33. Meng, B.; Feng, X.; Qiu, G.; Anderson, C.W.N.; Wang, J.; Zhao, L. Localization and speciation of mercury in brown rice with implications for pan-asian public health. *Environ. Sci. Technol.* **2014**, *48*, 7974–7981. [CrossRef] [PubMed]
34. Manceau, A. Comment on "direct observation of tetrahedrally coordinated fe(iii) in ferrihydrite". *Environ. Sci. Technol.* **2012**, *46*, 6882–6884. [CrossRef] [PubMed]
35. Manceau, A.; Enescu, M.; Simionovici, A.; Lanson, M.; Gonzalez-Rey, M.; Rovezzi, M.; Tucoulou, R.; Glatzel, P.; Nagy, K.L.; Bourdineaud, J.-P. Chemical forms of mercury in human hair reveal sources of exposure. *Environ. Sci. Technol.* **2016**, *50*, 10721–10729. [CrossRef] [PubMed]

36. Manceau, A.; Lemouchi, C.; Rovezzi, M.; Lanson, M.; Glatzel, P.; Nagy, K.L.; Gautier-Luneau, I.; Joly, Y.; Enescu, M. Structure, bonding, and stability of mercury complexes with thiolate and thioether ligands from high-resolution xanes spectroscopy and first-principles calculations. *Inorg. Chem.* **2015**, *54*, 11776–11791. [CrossRef] [PubMed]
37. Manceau, A.; Wang, J.; Rovezzi, M.; Glatzel, P.; Feng, X. Biogenesis of mercury–sulfur nanoparticles in plant leaves from atmospheric gaseous mercury. *Environ. Sci. Technol.* **2018**, *52*, 3935–3948. [CrossRef] [PubMed]
38. Driscoll, C.T.; Mason, R.P.; Chan, H.M.; Jacob, D.J.; Pirrone, N. Mercury as a global pollutant: Sources, pathways, and effects. *Environ. Sci. Technol.* **2013**, *47*, 4967–4983. [CrossRef] [PubMed]
39. Sun, S.; Kang, S.; Huang, J.; Chen, S.; Zhang, Q.; Guo, J.; Liu, W.; Neupane, B.; Qin, D. Distribution and variation of mercury in frozen soils of a high-altitude permafrost region on the northeastern margin of the tibetan plateau. *Environ. Sci. Pollut. Res.* **2017**, *24*, 15078–15088. [CrossRef] [PubMed]
40. Whiteside, M.; Herndon, J. Coal fly ash aerosol: Risk factor for lung cancer. *J. Adv. Med. Med. Res.* **2018**, *25*, 1–10. [CrossRef]
41. Yin, Y.; Xu, W.; Tan, Z.; Li, Y.; Wang, W.; Guo, X.; Yu, S.; Liu, J.; Jiang, G. Photo- and thermo-chemical transformation of agcl and ag2s in environmental matrices and its implication. *Environ. Pollut.* **2017**, *220*, 955–962. [CrossRef] [PubMed]
42. Tian, S.; Zhu, Y.; Meng, B.; Guan, J.; Nie, Z.; Die, Q.; Xu, W.; Yu, M.; Huang, Q. Chemical speciation of lead in secondary fly ash using X-ray absorption spectroscopy. *Chemosphere* **2018**, *197*, 362–366. [CrossRef] [PubMed]
43. Lieb-Lappen, R.M.; Golden, E.J.; Obbard, R.W. Metrics for interpreting the microstructure of sea ice using X-ray micro-computed tomography. *Cold Reg. Sci. Technol.* **2017**, *138*, 24–35. [CrossRef]
44. Lieblappen, R.M.; Kumar, D.D.; Pauls, S.D.; Obbard, R.W. A network model for characterizing brine channels in sea ice. *Cryosphere* **2018**, *12*, 1013–1026. [CrossRef]
45. Maus, S.; Huthwelker, T.; Enzmann, F.; M Miedaner, M.; Stampanoni, M.; Marone, F.; Hutterli, M.; Hintermüller, C.; Kersten, M. Synchrotron-based X-ray micro-tomography: Insights into sea ice microstructure. In Proceedings of the Sixth Workshop on Baltic Sea Ice Climate, Lammi Biological Station, Finland, 2008; 2009; Volume 61, pp. 28–45.
46. Faria, S.H.; Weikusat, I.; Azuma, N. The microstructure of polar ice. Part ii: State of the art. *J. Struct. Geol.* **2014**, *61*, 21–49. [CrossRef]
47. Murshed, M.M.; Klapp, S.A.; Enzmann, F.; Szeder, T.; Huthwelker, T.; Stampanoni, M.; Marone, F.; Hintermüller, C.; Bohrmann, G.; Kuhs, W.F.; et al. Natural gas hydrate investigations by synchrotron radiation X-ray cryo-tomographic microscopy (srxctm). *Geophys. Res. Lett.* **2008**, *35*. [CrossRef]
48. Takeya, S.; Honda, K.; Gotoh, Y.; Yoneyama, A.; Ueda, K.; Miyamoto, A.; Hondoh, T.; Hori, A.; Sun, D.; Ohmura, R.; et al. Diffraction-enhanced X-ray imaging under low-temperature conditions: Non-destructive observations of clathrate gas hydrates. *J. Synchrotron Radiat.* **2012**, *19*, 1038–1042. [CrossRef] [PubMed]
49. Yang, L.; Zhao, J.; Liu, W.; Li, Y.; Yang, M.; Song, Y. Microstructure observations of natural gas hydrate occurrence in porous media using microfocus X-ray computed tomography. *Energy Fuels* **2015**, *29*, 4835–4841. [CrossRef]
50. Arzbacher, S.; Petrasch, J.; Ostermann, A.; Loerting, T. Micro-tomographic investigation of ice and clathrate formation and decomposition under thermodynamic monitoring. *Materials* **2016**, *9*, 668. [CrossRef] [PubMed]
51. Koebernick, N.; Daly, K.R.; Keyes, S.D.; George, T.S.; Brown, L.K.; Raffan, A.; Cooper, L.J.; Naveed, M.; Bengough, A.G.; Sinclair, I.; et al. High-resolution synchrotron imaging shows that root hairs influence rhizosphere soil structure formation. *New Phytol.* **2017**, *216*, 124–135. [CrossRef] [PubMed]
52. Porra, L.; Dégrugilliers, L.; Broche, L.; Albu, G.; Strengell, S.; Suhonen, H.; Fodor, G.H.; Peták, F.; Suortti, P.; Habre, W.; et al. Quantitative imaging of regional aerosol deposition, lung ventilation and morphology by synchrotron radiation ct. *Sci. Rep.* **2018**, *8*, 3519. [CrossRef] [PubMed]
53. Bartels-Rausch, T. Ten things we need to know about ice and snow. *Nature* **2013**, *494*, 27–29. [CrossRef] [PubMed]
54. Bartels-Rausch, T.; Bergeron, V.; Cartwright, J.H.E.; Escribano, R.; Finney, J.L.; Grothe, H.; Gutiérrez, P.J.; Haapala, J.; Kuhs, W.F.; Pettersson, J.B.C.; et al. Ice structures, patterns, and processes: A view across the icefields. *Rev. Mod. Phys.* **2012**, *84*, 885–944. [CrossRef]
55. Nakamura, T.; Noguchi, T.; Tsuchiyama, A.; Ushikubo, T.; Kita, N.T.; Valley, J.W.; Zolensky, M.E.; Kakazu, Y.; Sakamoto, K.; Mashio, E.; et al. Chondrulelike objects in short-period comet 81p/wild 2. *Science* **2008**, *321*, 1664. [CrossRef] [PubMed]

56. Fitzner, M.; Sosso, G.C.; Cox, S.J.; Michaelides, A. The many faces of heterogeneous ice nucleation: Interplay between surface morphology and hydrophobicity. *J. Am. Chem. Soc.* **2015**, *137*, 13658–13669. [CrossRef] [PubMed]
57. Macis, S.; Cibin, G.; Maggi, V.; Baccolo, G.; Hampai, D.; Delmonte, B.; D'Elia, A.; Marcelli, A. Microdrop deposition technique: Preparation and characterization of diluted suspended particulate samples. *Condens. Matter* **2018**, *3*, 21. [CrossRef]
58. D'Elia, A.; Cibin, G.; Robbins, P.E.; Maggi, V.; Marcelli, A. Design and characterization of a mapping device optimized to collect xrd patterns from highly inhomogeneous and low density powder samples. *Nucl. Instrum. Methods Phys. Res. Sec. B Beam Interact. Mater. Atoms* **2017**, *411*, 22–28. [CrossRef]
59. From glacier to climate—Euro-Asian perspectives in cryospheric sciences. In Proceedings of the Bilateral Chinese/Italian Workshop, Beijing, China, 9–10 July 2012.
60. Shen, X.; Sun, L.; Zhang, L.; Yin, X.; Kang, S.; Wu, Z.; Ju, X.; Huang, Y. Analysis on the 6 species of alagae and lichen by sr-xrf in the fileds peninsula of antarctica. *Chin. J. Pol. Res.* **2001**, *13*, 187–194.
61. Shen, X.; Sun, L.; Yin, X.; Zhang, L.; Kang, S.; Wu, Z.; Huang, Y.; Ju, X. X-ray fluorescent analysis of the 6 species of bryophyte in the king george iland, antarctica. *Chin. J. Pol. Res.* **2001**, *13*, 50–56.
62. Xie, Z.; Sun, L.; Long, N.; Li, Z.; Kang, S.; Wu, Z.; Huang, Y.; Xin, J. Analysis of the distribution of chemical elements in adelie penguin bone using synchrotron radiation X-ray fluorescence. *Pol. Biol.* **2003**, *26*, 171–177.
63. Xie, Z.; Sun, L.; Blum, J.D.; Huang, Y.; He, W. Summertime aerosol chemical components in the marine boundary layer of the arctic ocean. *J. Geophys. Rese. Atmos.* **2006**, *111*. [CrossRef]
64. Liao, J.; Huey, L.G.; Liu, Z.; Tanner, D.J.; Cantrell, C.A.; Orlando, J.J.; Flocke, F.M.; Shepson, P.B.; Weinheimer, A.J.; Hall, S.R.; et al. High levels of molecular chlorine in the arctic atmosphere. *Nat. Geosci.* **2014**, *7*, 91–94. [CrossRef]
65. Shi, Z.; Krom, M.D.; Jickells, T.D.; Bonneville, S.; Carslaw, K.S.; Mihalopoulos, N.; Baker, A.R.; Benning, L.G. Impacts on iron solubility in the mineral dust by processes in the source region and the atmosphere: A review. *Aeolian Res.* **2012**, *5*, 21–42. [CrossRef]
66. Domine, F.; Cincinelli, A.; Bonnaud, E.; Martellini, T.; Picaud, S. Adsorption of phenanthrene on natural snow. *Environ. Sci. Technol.* **2007**, *41*, 6033–6038. [CrossRef] [PubMed]
67. Schroeder, W.H.; Anlauf, K.G.; Barrie, L.A.; Lu, J.Y.; Steffen, A.; Schneeberger, D.R.; Berg, T. Arctic springtime depletion of mercury. *Nature* **1998**, *394*, 331. [CrossRef]
68. Jitaru, P.; Gabrielli, P.; Marteel, A.; Plane, J.M.C.; Planchon, F.A.M.; Gauchard, P.-A.; Ferrari, C.P.; Boutron, C.F.; Adams, F.C.; Hong, S.; et al. Atmospheric depletion of mercury over antarctica during glacial periods. *Nat. Geosci.* **2009**, *2*, 505–508. [CrossRef]
69. Jeong, D.; Kim, K.; Choi, W. Accelerated dissolution of iron oxides in ice. *Atmos. Chem. Phys.* **2012**, *12*, 11125–11133. [CrossRef]
70. Pratt, K.A.; DeMott, P.J.; French, J.R.; Wang, Z.; Westphal, D.L.; Heymsfield, A.J.; Twohy, C.H.; Prenni, A.J.; Prather, K.A. In situ detection of biological particles in cloud ice-crystals. *Nat. Geosci.* **2009**, *2*, 398–401. [CrossRef]
71. Marcelli, A.; Maggi, V. *Aerosols in Snow and Ice. Markers of Environmental Pollution and Climatic Changes: European and Asian Perspectives*; Superstripes Press: Rome, Italy, 2017.
72. Marcelli, A. The large research infrastructures of the people's republic of china: An investment for science and technology. *Phys. Status Solidi (B)* **2013**, *251*, 1158–1168. [CrossRef]